ISSN 1349-1121
JAXA-RM-06-016E

JAXA Research and Development Memorandum

Chemiluminescence sensor for active control of combustion

Laurent ZIMMER , Shigeru TACHIBANA

March 2007

Japan Aerospace Exploration Agency

This document is provided by JAXA.

This document is provided by JAXA.

Chemiluminescence sensor for active control of combustion

Laurent ZIMMER and Shigeru TACHIBANA
Aeroengine Technnology Center, Institute of Aerospace Technology, JAXA

Abstract

The present document summarizes the different experiments done on active control by using chemiluminescence measurements. First a brief introduction on the chemical mechanisms that are responsible for chemiluminescence in hydrocarbon flames is presented together with simulations for lean cases. Detailed discussion and limitations of inverse Abel transform to estimate the planar distribution of the chemiluminescence is shown, and effects of absorption and geometrical optics are discussed. A brief presentation of the two different combustors is done followed by a detailed explanation of the results obtained with chemiluminescence. Three different chemiluminescence techniques are used, namely spatially, spectrally and temporally resolved techniques. All those three approaches prove to be useful to characterize the oscillating mechanisms occurring in premixed combustors. Imaging techniques are used to show the regions where strong coupling between pressure and heat release exist. Spectrally resolved techniques are used to discuss the nature of the flame (from premixed to non fully premixed) and to obtain an estimate of the equivalence ratio through emission ratio between OH^* and CH^* emissions. Finally, temporally resolved techniques can be used to detect onset of oscillatory combustion using combined pressure-chemiluminescence product or through an analysis in the frequency domain (coherence) to understand the frequencies at which coupling between pressure and heat release occurs. Conclusions are drawn and emphasizes for future investigations are addressed.

1 Introduction

Reducing nitric oxides (NOx) from engines is becoming a crucial issues in many important areas. One way to achieve drastic reduction of NOx is to use lean premixed combustion, rather than non-premixed types. With a lower flame temperature, NOx can effectively be reduced. However, two possibly harmful effects have to be considered. The first one is the possibility to have thermo-acoustic oscillations occurring, for which heat release and pressure would be in phase (see [1] for a recent review on the phenomena). The second one is the blow-out of the flame, as target stoichiometry would be ideally very close to blow-off, to reduce as much as possible flame temperature. When dealing with active control strategies, the definition of the proper quantities to measure is very important [2].

This document is provided by JAXA.

For purely aero-acoustics problems, pressure sensors are well suited ([3]) and a typical actuator may be a loudspeaker. However combustion involves also heat release and chemical reactions and it seems possible to take benefit from this aspect to include other sensing and actuating devices. Due to the harsh environment inside a combustor, intrusive techniques (such as gas sampling) may not be an adequate choice in control loop strategies, as their temporal reliability may not be very high. Despite these considerations, it may be useful in some small-scales turbines for developing active control strategies ([4]). Non-intrusive techniques may however require an external input (such as the case for DLAS techniques as presented in ([5],[6]) which requires a laser at high repetition rate or requires scanning over some wavelength). This solution may not be adequate for long time use in gas turbines and one may look towards natural emission of light through chemical reactions (chemiluminescence) as being a good candidate for sensing purpose.

For combustion control, the harsh environment increases the difficulties. The monitored quantities have to be mainly influenced by combustion kinetics rather than other phenomenon. A recent review of the different possibilities has recently been proposed [7]. In the present context, only chemiluminescence will be investigated and the different solutions existing when using chemiluminescence for active control of combustion will be addressed.

Section 2 will present the origin of chemiluminescence as well as simulations using latest chemical mechanisms. Section 3 will give a detailed description of the measurement techniques. Section 4 will discuss in details the inverse Abel transformation, used to retrieve planar emission from three-dimensionally averaged emission. Section 5 will be used to present the experimental facilities. Afterwards Section 6 will be devoted to the results obtained using spatially, spectrally and finally temporally resolved techniques. Each approach will be illustrated by a series of examples. Conclusions will be drawn and suggestions for implementing chemiluminescence in active control loops will be made.

2 Origin of chemiluminescence

The exact origin of chemiluminescence is still under investigations ([8]). When dealing with hydrocarbons, three main species are identified in typical spectrum OH ($A^2\Sigma^+ - X^2\Pi$), CH ($A^2\Delta - X^2\Pi$) and C_2 ($d^3\Pi_g - a^3\Pi_u$). In the following of this paper, the excited state will be designated by an asterisk. The third species is mainly coming from relatively rich conditions. There exists different mechanisms to generate OH*, the main path being CH reactions with oxygen, whereas other paths exist for hydrogen combustion.

$$\begin{aligned} CH + O_2 &\rightarrow OH^* + CO \\ H + O + M &\rightarrow OH^* + M \\ H + 2OH &\rightarrow H_2O + OH^* \end{aligned} \tag{1}$$

The sources of CH* are coming from C_2H chemistry, as depicted by the following reactions:

This document is provided by JAXA.

$$C_2H + O \rightarrow CH^* + CO$$
$$C_2H + O_2 + M \rightarrow CH^* + CO_2 \quad (2)$$

C_2^* reactions are usually modeled by

$$CH_2 + C \rightarrow C_2^* + H_2 \quad (3)$$

De-excitation of the different molecules can be done by collisional quenching or emission of light (chemiluminescence). Those different mechanisms are modeled through an Arrhenius form which constants are taken from [8].

In the present case, simulations are done for equivalence ratio ranging from 0.40 to 1.40 and inlet temperature from 290K to 690K. Of course, a stable flame can not be achieved for leanest cases with ambient temperature conditions. Those computations are carried out using the numerical code PREMIX of Chemkin is used with the GRI-Mech3.0 mechanisms. A typical example of calculation of OH^* and CH^* is given in Figure 1(a) for an equivalence ratio of 0.40 and an inlet temperature of 690K in case of methane-air mixtures. The CH^* has been multiplied by 10 so that a similar scale as the one used for OH^* can be used. One can see that OH^* and CH^* are slightly shifted with respect to their maximum of temperature gradient. Peaks OH^* and CH^* coincide well, within all the ranges of equivalence ratio simulated, as for instance shown in Figure 1(b).

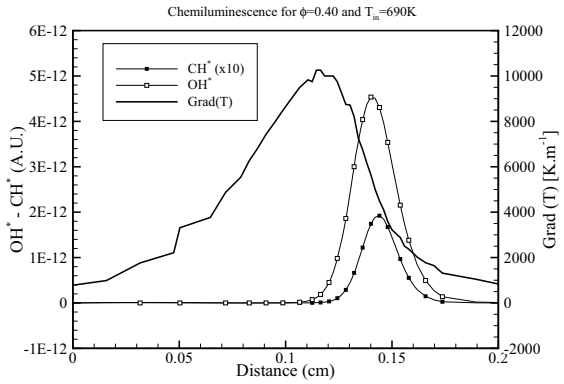

(a) Chemiluminescence peak versus gradient of temperature for methane-air premixed flame with $\phi = 0.40$

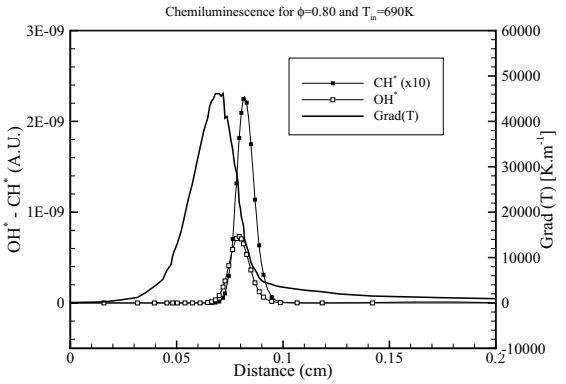

(b) Chemiluminescence peak versus gradient of temperature for methane-air premixed flame with $\phi = 0.80$

Figure 1: Difference between the peak of OH^*, the peak of CH^* and the gradient of temperature

The differences between the two peaks are summarized in Figure 2(a) for two different inlet temperatures and for equivalence ratio ranging from 0.4 to 0.9. One can see that an increase of inlet temperature tends to shift the peak of OH^* towards the unburned side for a similar equivalence ratio, as the distance between the maximum gradient of temperature and the peak of chemiluminescence is decreasing. One can

This document is provided by JAXA.

also see that typical values tend to be of the order of 0.05cm for the worst cases for ambient temperature and typically of the order of 0.02cm for preheated cases.

Using the results of those simulations, it is possible to compute the differences between OH* and OH. In many numerical simulations, a complete scheme for OH* is not included and therefore the only data accessible is the molecular OH. To enhance the differences between OH and OH*, the typical distance between the peak of OH* and the OH profile is computed and represented in Figure 2(b). One can see that typically OH appears before the chemiluminescence but that the differences remain relatively limited to a few hundreds of micrometers.

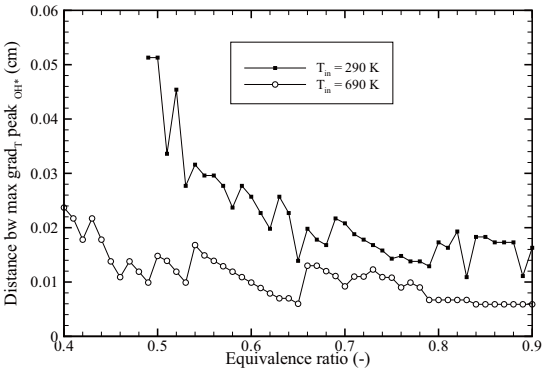

(a) Distance between peaks of chemiluminescence and peak of gradient of temperature as function of equivalence ratio for different inlet temperature (Methane-air flames)

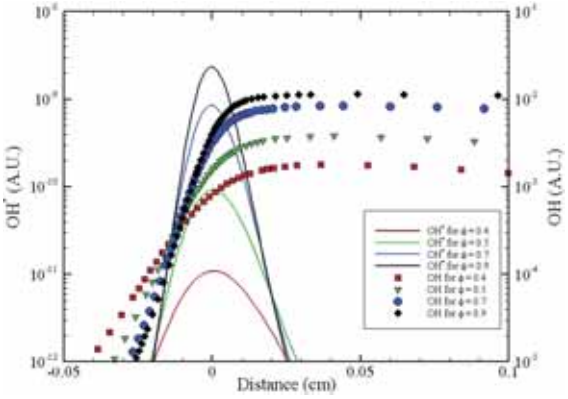

(b) Typical distance between peak of OH* (taken as reference distance) and OH profile for T_{in}=690K (Methane-air flames)

Figure 2: Distance between peaks of OH* and other quantities for methane-air premixed flames

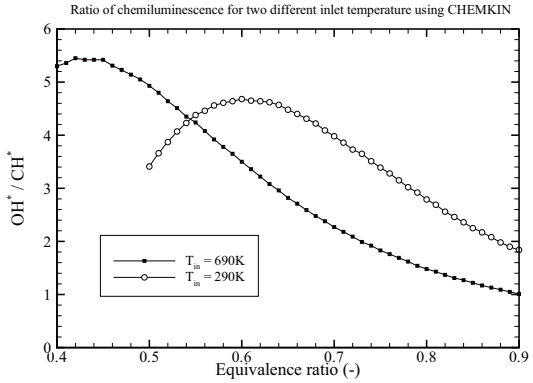

Figure 3: Variations of the ratio OH*/CH* with equivalence ratio and inlet temperature for premixed methane-air flames

Another interesting point obtained from those simulations, and that was not previously shown in other simulations ([8]), is the changes of the ratio between OH* and

This document is provided by JAXA.

CH^*, especially for lean conditions as shown in Figure 3. Many applications focus on equivalence ratio higher than 0.60 at ambient temperature (see for instance [9]) and therefore those changes were not shown previously.

Two important results can be seen. The first is that the ratio is not monotonic as a peak in the ratio is observed at an equivalence ratio of 0.60 for Tin=290K and at 0.43 for Tin=690K. The other very important information is that the inlet temperature has an important impact on the shape of both ratio and therefore using chemiluminescence as indicator of local stoichiometry requires careful examination of the experimental conditions. Simulations for ambient temperature were usually done for equivalence ratio higher than 0.70 and therefore this behavior was not shown ([8]). The decrease in the OH^*/CH^* ratio with an increase of stoichiometry comes from the increase of carbon content. It is worth noting that the decrease of this ratio occurs for stoichiometry around 0.60 below which flames can still be sustained. Therefore this may also occur in real cases and great care has to be taken when analyzing experimental data. The inversion occurs for stoichiometry around 0.42 for the preheated case.

The present simulations show that relative chemiluminescence for equivalence ratio measurements should be treated very carefully, especially for the lean side.

3 Measurement techniques

In this section, the different measurement techniques used are exposed.

3.1 Spectrometer

Prior to any other measurement techniques, detailed spectrometry should always be used in order to determine the exact origin of the chemiluminescence. The light emitted at some wavelength is coming from the superposition of emission due to a narrow-band molecule (like OH^*, CH^*), to the emission of broad-band molecules (like CO_2) and to background emission, some of which may come from black body radiation. Therefore, before affecting to OH^* all the intensity emitted around 306nm, it is very important to check that no other source of emission exists.

For those kinds of experiments, a spectrometer, coupled to an ICCD camera is used. The collecting light probe is a lens with focal length of 300mm coupled to a fiber optics. The fiber optics is connected to a spectrometer (MS-257 from Oriel) and measurements are made with an ICCD (Andor) with a slit of 50μm. The spectral resolution is 0.33nm when using 150/300 gratings. This resolution is good enough as well-known transitions are measured.

3.2 Specbox

When oscillation frequencies are of interest another type of measurement technique is used. For temporally resolved acquisition, the light is provided through a series of dichroic mirrors and band pass filters to high-sensitivity photo-multipliers (as shown in Figure 4).

The dichroic mirrors are made such as reflecting only a small part of the spectrum centered on the bandwidth of the band-pass filter. Typical acquisition frequency is

This document is provided by JAXA.

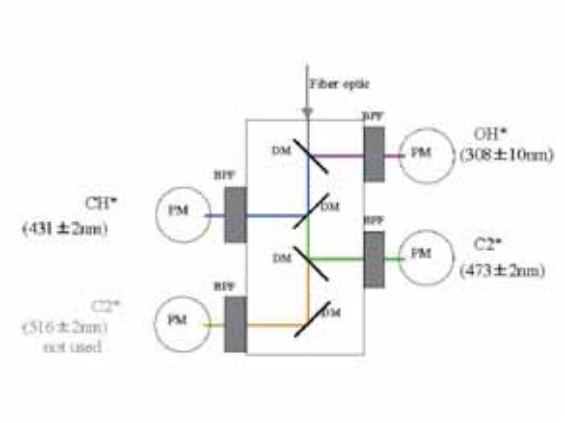

Figure 4: Skecth of the series of mirrors, filters and photo-multipliers

between 10kHz and 50kHz. Table 1 summarizes the different wavelength monitored and the main species corresponding to this emission.

Emission	308± 10nm	431± 2nm	473±2nm
Radical	OH^*	CH^*	C_2^* or CO_2^*

Table 1: Wavelength monitored and corresponding radicals

It is worth noting that usually the third wavelength is used to measure C_2^*. However, it is known that in lean flames, C_2^* is very weak and can be negligible compared to CO_2^* ([10]). This arrangement allows a simultaneous measurement of those species at a high acquisition frequency (with a maximum rate of 50kHz). One advantage of chemiluminescence compared to pressure sensor is that measurement locations can be easily changed if proper optical access is available. The pressure sensors (Kulite Semiconductor Products, Inc., Model XTL-190-15G) are used with the technique of the semi-infinite tube to avoid spurious signals ([11]).

3.3 Intensified cameras

To have some spatial resolution, chemiluminescence is also acquired with ICCD. For OH^* measurements, a combination of Schott-UG5 and WG305 is used. UG5 aims at removing emission between 400nm and 600nm while WG305 aims at removing emission below 290nm. This latter is useful when applying Planar Laser Induced Fluorescence on the OH molecule for which the excitation wavelength is around 283nm. Light emitted above 600nm is also imaged, but in lean premixed methane-air flames, mainly light from OH^* is gathered by this method. Band-pass filters are available for 306nm but the resultant transmission is relatively small and this combined UG5-WG305 shall give a higher signal to noise ratio. As for CH^* measurements, a band-pass filter centered around 430nm is used.

The ICCD used in the present case is a 384×576 pixels, 12 bits camera. The exposure time can be controlled to within a few microseconds and gain can be adjusted

This document is provided by JAXA.

in hardware. No simultaneous measurements of OH^* and CH^* is used in the present case.

This section introduced the different measurement techniques available when dealing with chemiluminescence. Next sections will show the way to treat the data and the advantages of the different approaches.

4 Abel transform

When acquiring chemiluminescence through a camera, one gathers the overall light. To have an estimation of the emission from a plane, one has to use some inversion scheme. A study ([12]) showed that the best algorithm with respect to noise is a three points Abel inversion, whereas onion-peeling algorithms have a noise value twice as the ones of the three points Abel, but equivalent to a two points Abel transform. Whatever the algorithm selected, some issues have first to be presented to understand the limitations of such approaches, as far as real experiments are concerned.

4.1 Mathematical description of Abel transform

Let $f(r)$ be a function that is axi-symmetric. To obtain the value of $F(x)$, which corresponds to the value of the projection of $f(r)$ onto a plane

$$F(x) = 2\int_x^\infty \frac{f(r)dr}{\sqrt{r^2 - x^2}} \tag{4}$$

To have the inverse of the transform, one starts from $(F(x))$ (like in real application, when one has the chemiluminescence signal) and one retrieves the value of $f(r)$ using

$$f(r) = -\frac{1}{\pi}\int_r^\infty \frac{dF}{dx}\frac{dx}{\sqrt{x^2 - r^2}} \tag{5}$$

4.2 Without noise and without absorption

This is the ideal case. This approach allows to check the validity of the developed software. At first, a simple doughnut like emission is considered. Signal is always positive and negative values arising from those equations are set to zero. In the following, X,Y as well as the chemiluminescence signal will be presented without units.

$$\begin{aligned} d_0 &= 2 + Y/50 \times 6 \\ signal &= \exp(1) - \exp((d_0 - r)^2/2) \end{aligned} \tag{6}$$

where d_0 is the position for which emission is the strongest within a vertical plane, Y is the streamwise position. In the following, only half of the domain is considered as axi-symmetry exists. To create the image of the chemiluminescence as seen by a virtual camera, the entire domain is simulated (X,Y,Z) and the intensity of pixels are summed up along rows (Z) to give the intensity as seen by each pixel (X,Y). The procedure is repeated for a different height (Y). A typical true planar distribution of the simulated signal is represented in Figure 5(a) with its three dimensional integrated

This document is provided by JAXA.

result shown in Figure 5(b). One can for instance observe that even though the peak signal is constant in the planar profile, values close to the exit are much lower than those measured further downstream. This is an important fact to understand and keep in mind when analyzing measurements done with chemiluminescence.

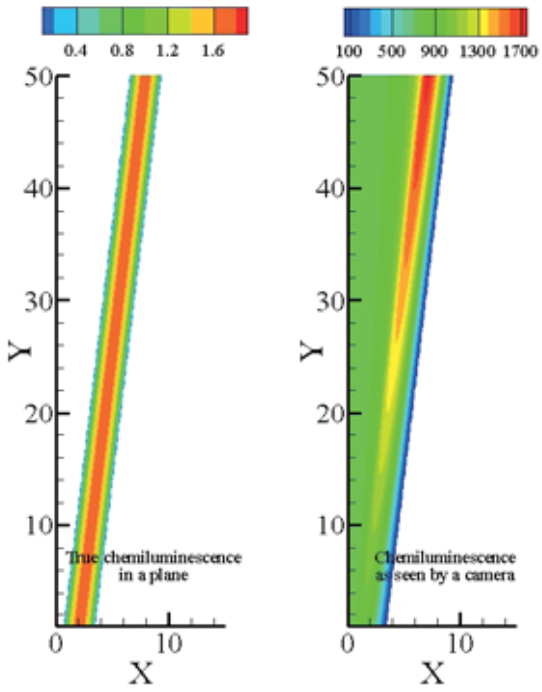

(a) True planar chemiluminescence distribution simulated

(b) Integration of planar information to yield Abel transform data

Figure 5: Presentation of test case 1 for Abel inverse transform without noise and without absorption.

To better compare the effectiveness of the inverse Abel transform, two profiles are taken, one at Y=10 (Figure 6(a)) and the other one at Y=40 (Figure 6(b)). One can clearly notice that the peak of emission is well retrieved when applying inverse Abel transform and that the thickness of the actual "flame front" is also recovered. Of course, this case being for a simulation without noise is an ideal case.

Some flames may have a double structure (as reported in [13]). It may also be the case of a pilot supported combustor, with an inner flame coming from pilot combustion and the outer flame from the main combustion. Therefore, it is important to verify that Abel inversion is able to find such a double peak and to see also the typical uncertainties associated with those cases. Together with previous equations, a new emission is given by

$$signal = \exp(1) - \exp((d_0/2 - r)^2/2) \tag{7}$$

This document is provided by JAXA.

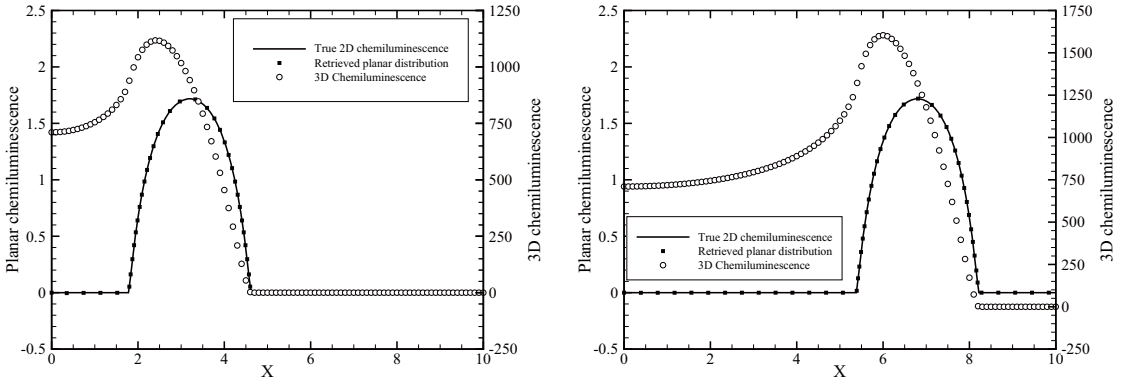

(a) Profile at Y=10

(b) Profile at Y=40

Figure 6: Comparisons between true profile and results obtained through inverse Abel transform for test case 1

Typical planar images are given in Figure 7(a) for true distribution and in Figure 7(b) for integrated results. The integrated results show a stronger signal in the inner side of the flame, even though the signal was equivalent for the inner and outer flame. This emphasizes the fact that analyzing integrated results tend to provide wrong views of actual phenomena.

In the case of a double structure, the intensity retrieved for a height Y of 10 and of 40 is shown in Figure 8(a) and 8(b) respectively. One can see that the outer part of the signal is properly retrieved. The peak coincides with the imposed peak. However, some discrepancies appear as far as inner peak is concerned. Results are also more noisy. Therefore, in case of pilot supported flame, one has to be careful with the findings of the inner flame and treat them with a greater care than those of simple flame or than the outer flame in the double-structure case. However, the intensity of both inner and outer are correctly reproduced, which allows a possible interpretation on the dynamics inside the combustor.

4.3 Effects of absorption

To see the effects that absorption of chemiluminescence may have on the Abel inversion, different absorption laws have been tested. Absorption may come from several reason, the biggest being some liquid jets like in cryogenic flames. The first law is to say that radiation may be blocked by liquid jets. A simple law of absorption is used:

$$absorption \propto (1 - \frac{X}{D_{\mathrm{LOx}}}) \tag{8}$$

In the above equation, D_{LOx} corresponds to the radius below which all radiation is considered as blocked. To model the signal as seen by a camera, one can not use the Abel transform. Instead, a complete computation of the intensity in 3D is done and the projection is done by considering absorption for the region behind the liquid jet. The radius of the jet is $D_{\mathrm{LOx}} = 3.2$ for Y=10 and $D_{\mathrm{LOx}} = 5.6$ for Y=30. Results of

This document is provided by JAXA.

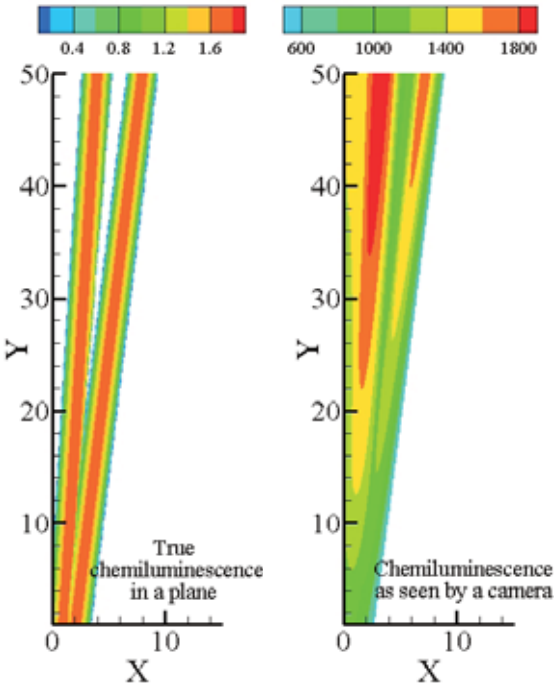

(a) True planar chemiluminescence distribution

(b) Integration of planar information to yield Abel transform data

Figure 7: Presentation of test case 2 for Abel inverse transform for a double flame, without noise and without absorption

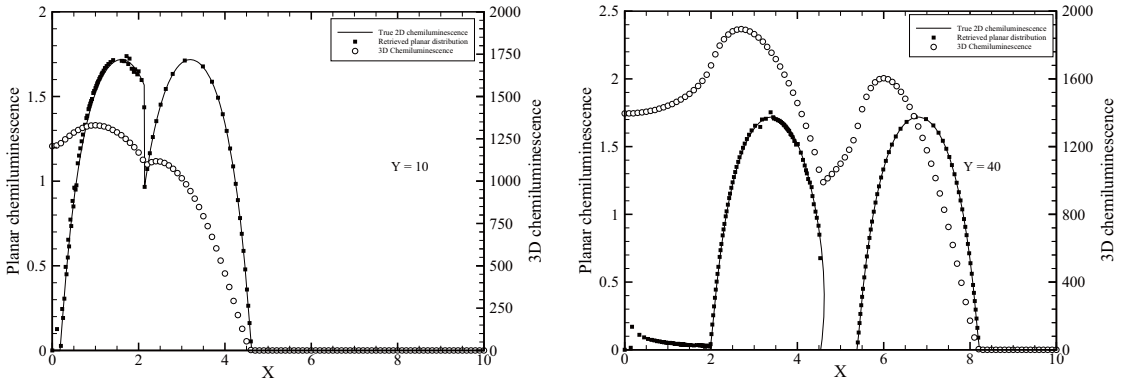

(a) Profile at Y=10

(b) Profile at Y=40

Figure 8: Comparisons between true profile and results obtained through inverse Abel transform for test case 2

This document is provided by JAXA.

the chemiluminescence profile at Y=10 and Y=30 are displayed in Figure 9. One can see that the inverse Abel transform becomes negative for radius smaller than 3.15 for Y=10 and smaller than 5.5. Those limits correspond indeed to the outer part of the liquid column.

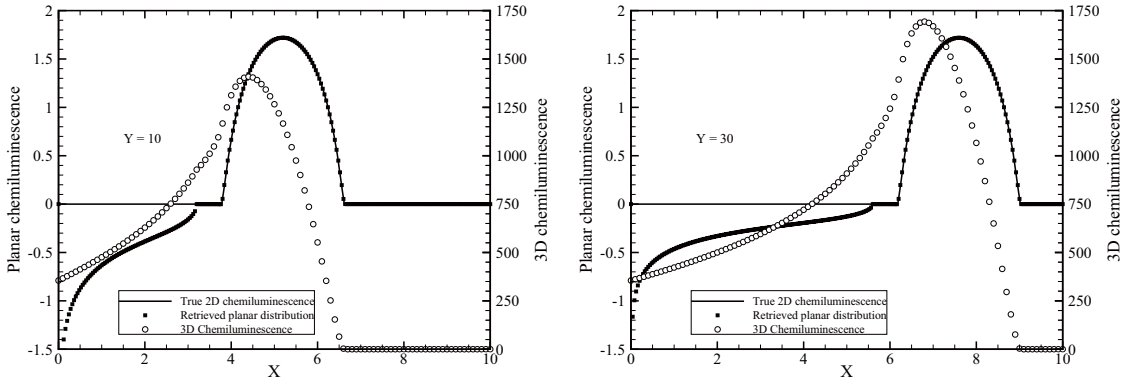

(a) Profile at Y=10

(b) Profile at Y=30

Figure 9: Comparisons between true profile and results obtained through inverse Abel transform for test case 3 with linear absorption from an inner liquid jet

Of course, in practice, the detection of negative chemiluminescence signal may not only result from absorption, but also from a non-symmetric pattern or noise. The effects of noise may be lowered by using filtering techniques on the images, like low-pass filters to remove high-frequency noise.

4.4 Effects of lens used

Another important issue when applying inverse Abel algorithm is that the actual rays of lights are not exactly parallel with respect to the imaging plane. To evaluate the differences, simulations are carried using a complete 3D description of the flame coupled to optical geometry to compute the actual emission capture by each different pixel. The present case will evaluate different distances of the camera from the center of the flame and different camera resolutions, matching the experimental characteristics of the intensified camera that will be used afterwards. However, to avoid complete description of the lenses, spherical lens approximation is used.

Table 2 summarizes the effects of the lens on the angular resolution achieved. Using a lens of 200mm will enable to have a limited field of view ($12°20'$) and therefore the working distance may be increased. The working distance reported in Table 2 is a relative working distance to capture an object of size 1 (used hereafter for normalization). One can see that a 50mm lens would require a very small working distance.

The pixels of the camera are considered as being a unique point compared to the distance with respect to the flame, whatever the lens used. The problem simulated is depicted in Figure 10.

The parameters investigated will first be the ratio between the distance from the camera and the centre of the flame to the diameter of the flame. This first parameter

This document is provided by JAXA.

Lens	50mm	105mm	200mm
Angle	46°	23°20′	12°20′
Distance	2.35	4.84	9.26

Table 2: Angular dispersion as function of lens

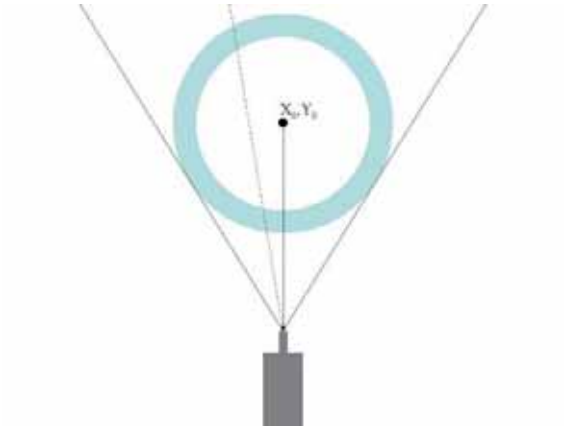

Figure 10: Sketch of the Simulation of a true chemiluminescence signal as seen by a camera

will be called *distance*. This parameter depends on the focal length of the lens used and therefore when presenting results, the focal length will be used. All illustration will be done with an axis between 0 and 1, 0 representing the center of the simulated camera and 1 the highest pixel number. Therefore, the represented pixel number will be half of the simulated one, the other half not being displayed due to symmetry. The lines along which integration is performed for the 100th pixel out of 384 is displayed in Figure 11. In this graph, an ideal case would correspond to a vertical line. One can see that a big difference arises for the 50mm case.

This is further illustrated in the profile of the recorded chemiluminescence, the effects of the focal length is represented in Figure 12(a). One can clearly see the differences in the profiles between a lens of 50mm and 105mm. Differences tend to decrease for lenses with focal length higher than 105mm. A distance of 10,000 is also simulated as being the ideal case and therefore is shown as being ∞.

The planar profiles retrieved from those different measurements are shown in Figure 12(b). One can clearly see that a 50mm lens would give a result slightly different from the other cases in both the position of the peak as well as the width of the distribution. This may have some consequences when analyzing the measurements and therefore, 50mm focal length should not be used when performing inverse Abel transform.

Even though, Abel transform seems straightforward, many effects have to be taken into account to be really able to propose semi-quantitative data from a 3D distribution. The effects on actual configurations on the uncertainties being qualified, one may proceed to the application of this inverse Abel scheme.

This document is provided by JAXA.

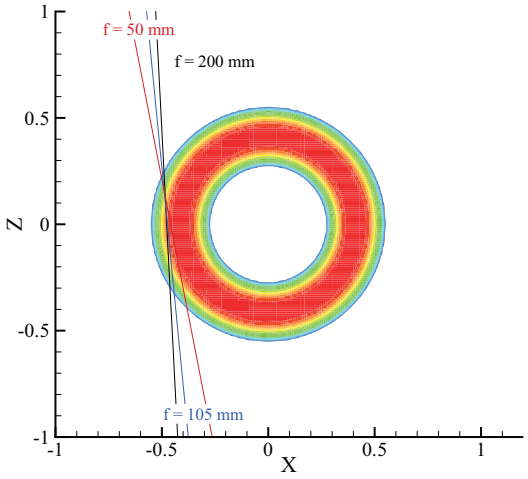

Figure 11: Differences in integration line as function of focal length. Ray tracing as seen by the 100^{th} pixel out of 384 pixels

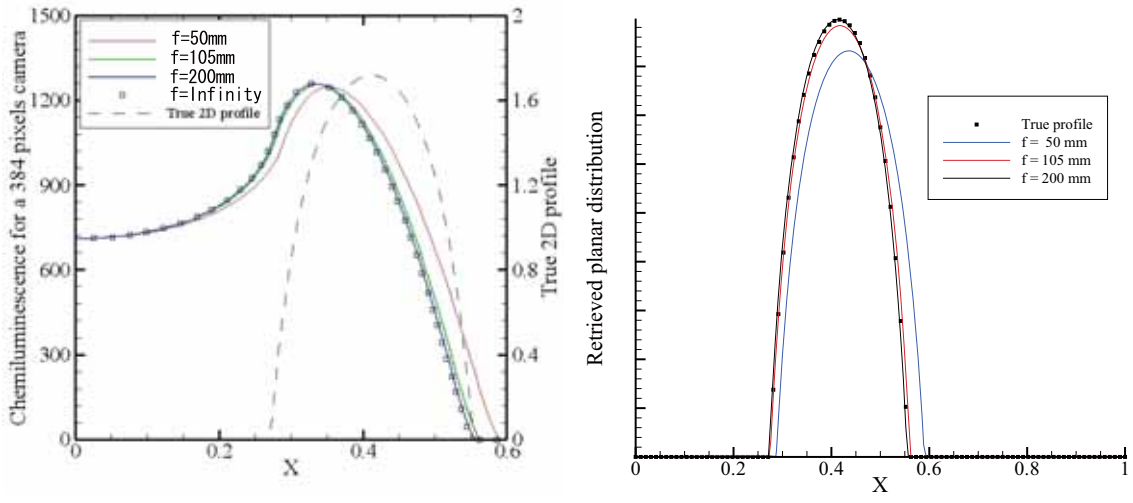

(a) Differences in signal seen by the camera (384 pixels) as function of focal length compared to an ideal case.

(b) Comparisons between the different planar information retrieved as function of focal length.

Figure 12: Effects of lens focal length on chemiluminescence profiles

This document is provided by JAXA.

5 Combustors

In the following, two different combustor will be alternatively used to show the utility of chemiluminescence in active control loop. Both combustor run with lean premixed methane-air at atmospheric pressure. The main differences reside in the pressure levels achieved for the natural oscillating mode as well as the adiabatic temperature of the flame (equivalence ratio) at which strong oscillations occurred. Both combustors have identical mixing chamber.

5.1 Swirler without recess

The first combustor (see Figure 13) has an overall length of 810mm. The outer and inner diameters of the swirler are respectively 50 and 20mm and is composed of 12 vanes of 30 degree angle. The inlet temperature is set to 500K with an overall mass flow rate of 60 g·s^{-1}. Strong oscillations occur for equivalence ratio laying between 0.65 and 0.85. Typical pressure fluctuations (see Figure 14) are around 0.75 to 1.2 kPa and subsequent frequencies are found around 200Hz. The emission index is measured at two different positions (at the exit of the combustor and 100mm inside the combustor).

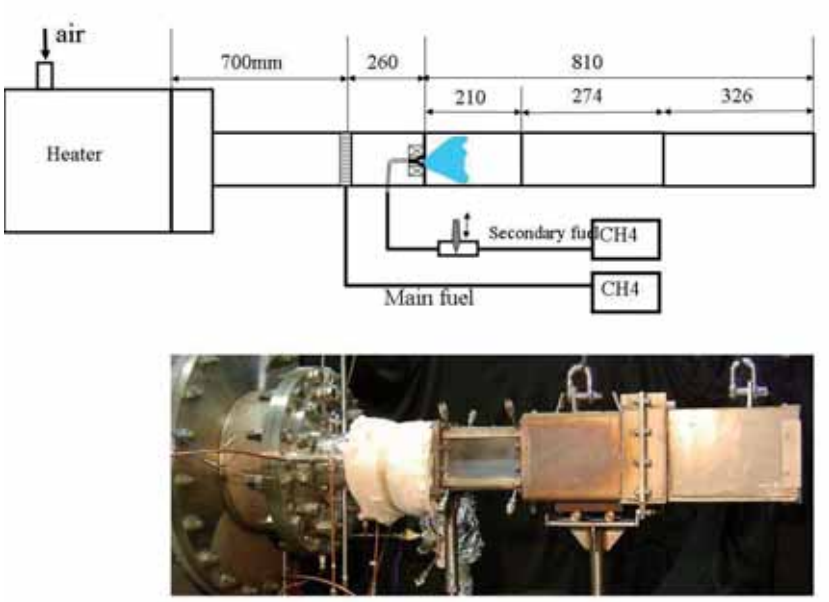

Figure 13: First setup used to evaluate chemiluminescence

5.2 Swirler with recess

The second combustor (see Figure 15) is run at 700K with a mass flow rate of 78 g·s^{-1} for the air (or a total flow rate of 1500Nl/min). The overall equivalence ratio studied caries between 0.43 and 0.60, which corresponds to adiabatic temperature between 1660 and 1960K. The first part of the combustor (up to 210mm downstream the swirl) is composed of four quartz to allow complete optical access. The second part (420mm long) consists of water-cooled stainless plate. The chemiluminescence measurements

This document is provided by JAXA.

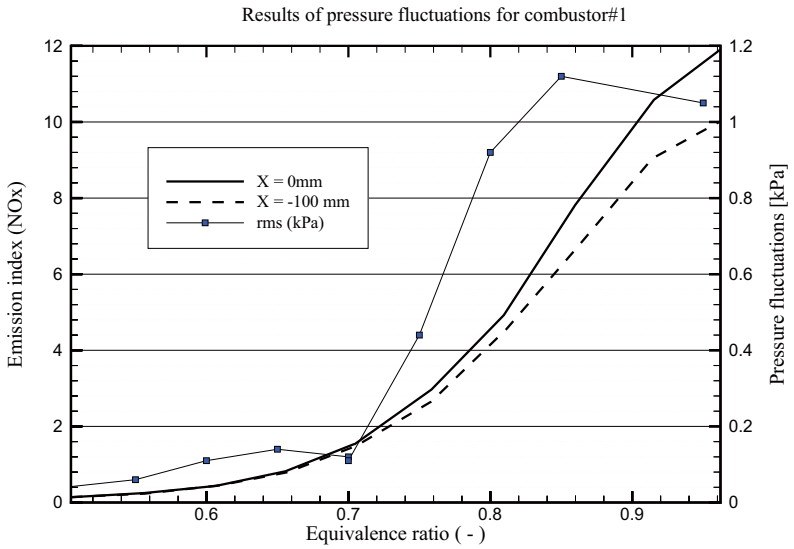

Figure 14: Characteristics of the combustor#1 in terms of pressure levels and emission index

have been taken in the first section, using either a simple fiber to get complete view of the section or a dual lens system in order to spatially limit the zone of interest. Both approaches provide slightly different data and they are examined in the next sections. The pressure sensor (Kulite Semiconductor Products, Inc., Model XTL-190-15G, located 10mm from the exit of the swirl) as well as the time series chemiluminescence are acquired simultaneously through a multi-channel data acquisition system (ONO SOKKI, DS-200, Graduo). Typical sampling frequency is 25.6kHz for each channel. The pilot injection is referred as percentage versus the total fuel injected. If one refers to the main mixture's injection, this would lead to a value of 0.2%.

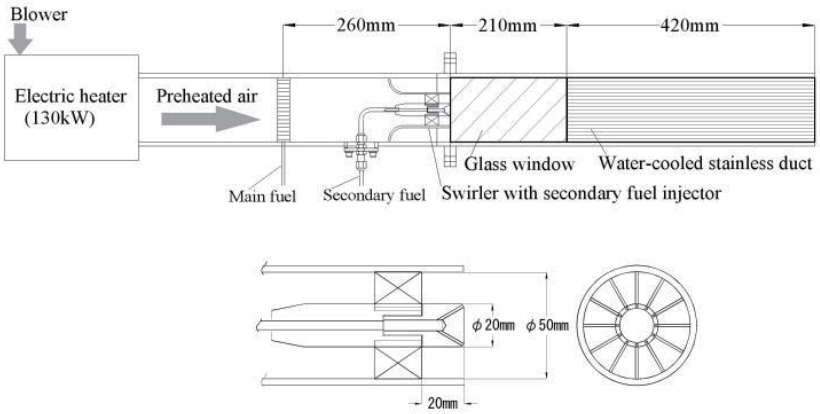

Figure 15: Sketch of the combustor #2

The typical pressure observed for over different equivalence ratio of (from $\phi = 0.43$ to 0.65 is displayed in Figure 16. The subsequent emission index of both NOx and CO is displayed in Figure 17. One can see that typical low emissions can be achieved for

This document is provided by JAXA.

overall equivalence ratio around 0.50 and that this value corresponds to the peak of pressures.

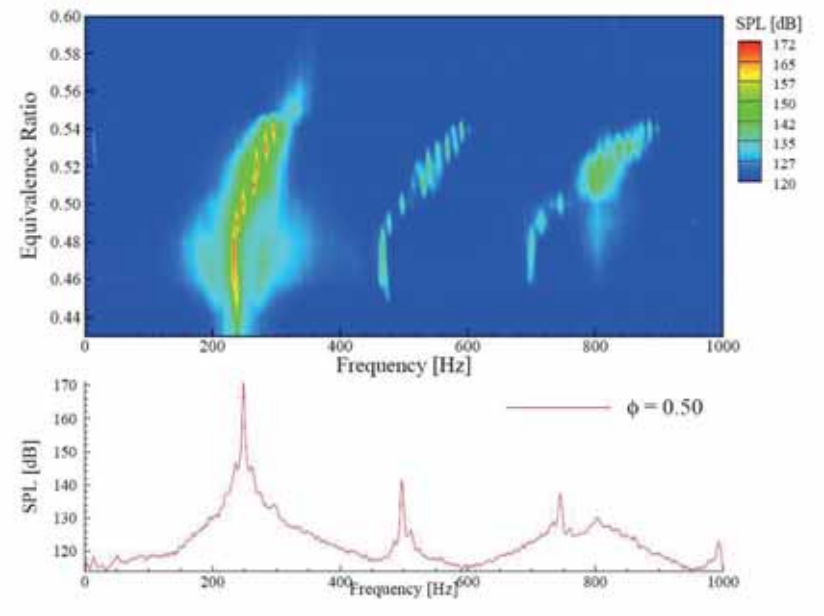

Figure 16: Pressure spectra for equivalence ratio ranging between $\phi = 0.43$ and 0.65

This is therefore considered as a setup typically representing the main problems in actual gas turbines: running in stoichiometry close to the blow-off to reduced emission may induce spurious pressure oscillations. To fully understand the nature of those oscillations and propose strategies to control them, chemiluminescence is used through imaging systems, by spectrally resolved measurements to give some hints about chemical reactions and by temporally resolved to show coherent behavior between pressure and chemiluminescence emission.

This document is provided by JAXA.

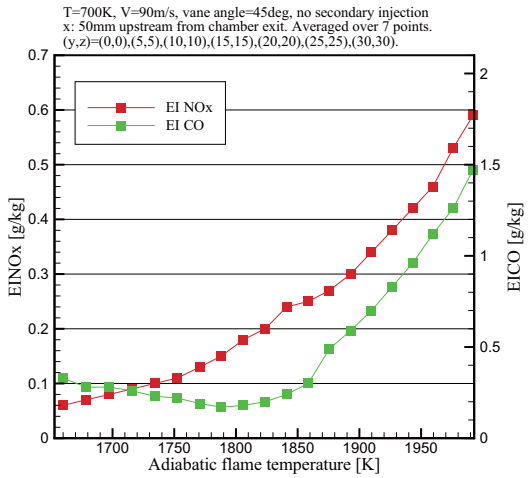

Figure 17: Emission index of NOx and CO for equivalence ratio ranging between $\phi = 0.43$ and 0.65

This document is provided by JAXA.

6 Results with imaging approach

For active control, the imaging techniques may lack of frequency response. Some alternatives may be found in linear photodiode arrays, like proposed in [14] to have both a temporal and spatial resolution. In the present case, standard intensified cameras are used. The objectives is to provide a spatial description of the flame dynamics, through the computations of a Rayleigh index map to enhance regions for which the coupling between heat release and pressure oscillations is strong.

Oscillating combustion is characterized by peak pressures that usually are easily measured. The frequency of the phenomena being relatively constant, the triggering of external measurements like phase-locked chemiluminescence images can be done. In the present part, the results obtained by triggering the chemiluminescence acquisition as function of the pressure signal are presented. The reference for pressure signal will always be taken at the point for which the signal is zero with a positive slope.

6.1 Visualization of flame structure

To better understand the mechanisms of oscillating combustion, phase-locked images of chemiluminescent emissions in case of oscillations are recorded. The pressure transducer is located at X = 20mm and Y = 0mm. The global chemiluminescence of OH^* is recorded as function of the phase delay with respect to the pressure signal. For that purpose, an ICCD (Princeton Instruments 576G/1) is used to capture the images of OH^*, with an UV-Nikkor 105mm/f4.5 lens. Its resolution is 576 by 384 pixels and typical measured area were 75mm×50mm, which gives a magnification 0.13 mm^2/pixel. It is used in gate mode with an exposure of 40 μs and a f-number of 4.5. Typically 80 images are recorded at each phase angle (20 points in case of oscillating flames, 10 points otherwise). The phase is determined with respect to the zero-crossing event in the filtered pressure signal with a positive slope. The filter had a bandwidth of 10Hz centered around the desired frequency. An illustration of the different phases is given in Figure 18 as well as a typical pressure signal within the combustor.

The flow comes from left to right (see Figure 19-20) and the bulk velocity of $12 m \cdot s^{-1}$ for an inlet temperature of 500K, the length of the combustor being 810mm; the typical frequencies are around 220Hz. The overall equivalence ratio for the case in Figure 20 is 0.73 (see Table 3 for full details) for a fully premixed case. Background is removed from all images and levels lower than 1% of the maximum are removed also for clarity reason. The images correspond to volume integration as no Abel transform is applied. One can notice an influence on the flame shape as a function of pressure phase.

Case	ϕ	Pilot[%]	Frequency [Hz]	Pressure [kPa]
Figure 19	0.73	0	220	1.83
Figure 20	0.87	10	245	1.83

Table 3: Experimental conditions

For the case of $\phi = 0.73$ and a phase delay of 10°, the flame front close to the exit seems to be deformed by a vortex-like structure coming from the inside of supplying mixture (height Y between 10 and 25mm). For a phase of 45°, this behavior is emphasized with the same structure being detected. For a phase of 90°, which represents

This document is provided by JAXA.

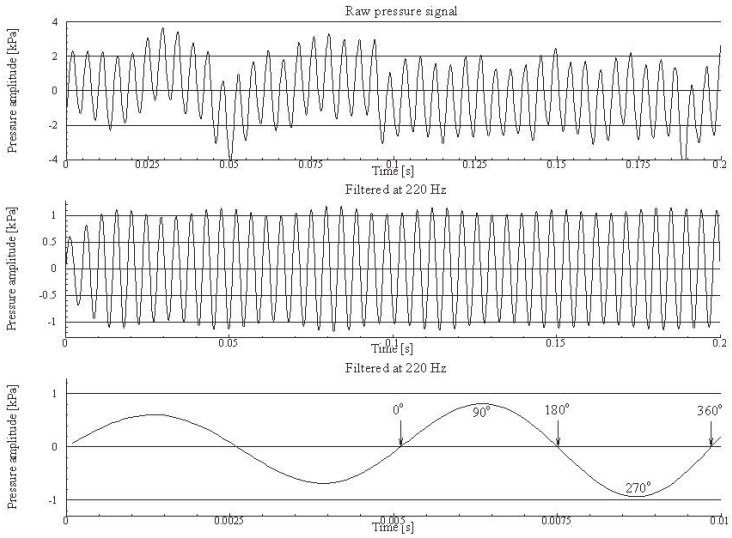

Figure 18: Raw and filtered pressure signal. Band-pass filter centered on the desired frequency is used.

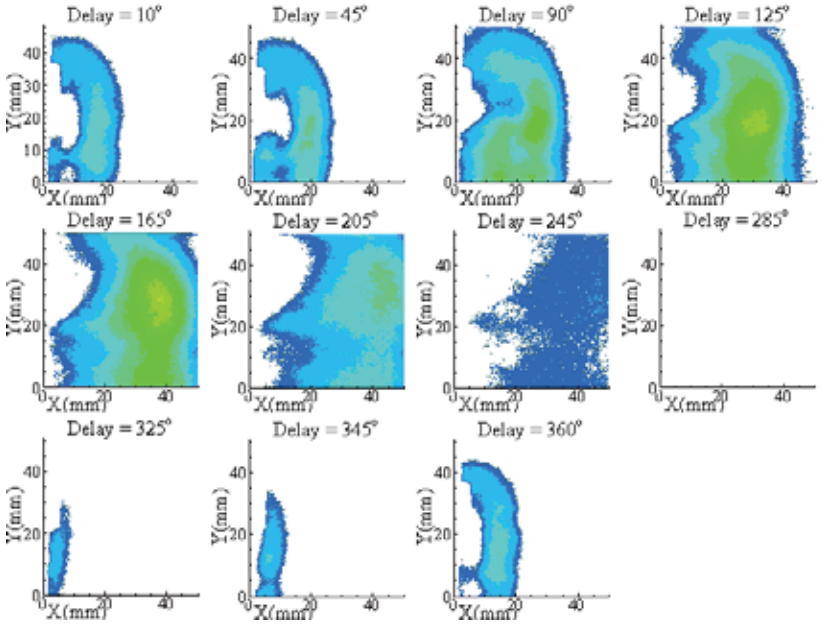

Figure 19: Phase-locked visualization of the unsteady process for premixed oscillating flame $\phi = 0.73$

This document is provided by JAXA.

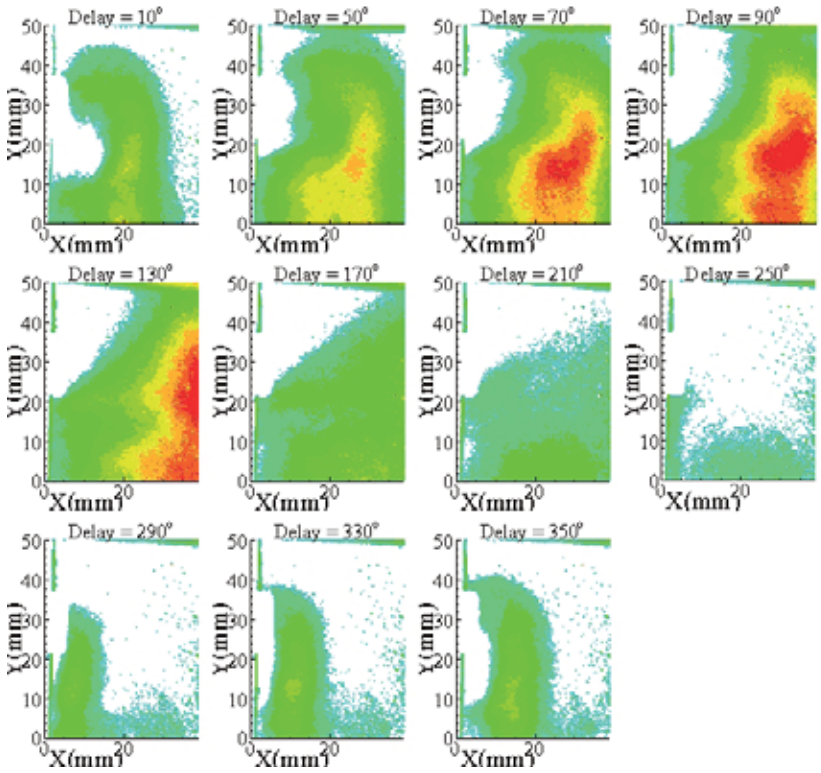

Figure 20: Phase-locked visualization of the unsteady process for partially premixed flame $\phi = 0.87$

This document is provided by JAXA.

the time where the pressure is at its maximum for a position of X=20mm along the centerline, the overall chemiluminescent emission increases. This increase is also seen for a phase delay of 125°, but at the position of the pressure probe (which is the line over which the chemiluminescent lens is integrated), one can notice that the emission diminishes. At this time, the outer part of the flame seems to be deformed whereas the central parts (for radial positions lower than 20mm) have a flat profile. For delays between 125° and 205°, one can notice that the boundaries as seen by the chemiluminescence seems to be moving with the mean flow, as typically low levels only can be found for temporal positions around 205° and 245°. The fact that no signal appears for a delay of 285° does not mean that the flame is completely lifted up or blown out, simply that the levels may be very small compared to background emission. What is more surprising are the results for delays after 300°, where a flame front is seen close to the exit of the swirler. It would have been more logical to see a flame front coming from the right side of the combustor (as for instance explained in [15]). Afterwards, this initial flame front develops and a vortex-like structure can be detected, as already mentioned for initial delays.

Somehow similar results can be found in case of secondary injection leading also to oscillating combustion (see Figure 20). The premixed remains unchanged but 10% of methane compared to the previous mixture is added and injected through small holes (1.4mm), placed inside the combustor. The overall equivalence ratio is in this case 0.87. Therefore, the overall chemiluminescence emission is higher for this case than the previous one. The secondary fuel is injected at 245Hz, with an opening time of 1.6ms and a phase delay of 190° compared to the pressure signal.The same mechanisms are present, even though the flame is not vanishing out of the measurement region. This may comes from higher equivalence ratio (hence higher signal to noise ratio). As can be seen for a phase delay of 250°, the central part exhibit chemiluminescent emission. This is an effect of secondary injection. This case leading to oscillations was a case for which the time delay between secondary injection and pressure was 2ms. Having a time lag of 72ms, this makes 74ms, resulting in a true phase shift of 160°, with an opening of 1.6ms, representing 65°.

6.2 Planar Rayleigh Index measurements

With the previous results, it is relatively hard to understand the true nature of the dynamics within the combustor. For a better image, one has to retrieve a planar information, using inverse Abel transform (see section 4). The present geometry having a square section, caution has to be made when dealing with results obtained close to the wall. In those regions, the axi-symmetry assuption is not valid. As stated in section 4, for practical cases, filters have first to be used to reduce the noise. A typical noise filtering is performed using low-pass filters with different kernel sizes. The kernel size is expressed in pixels and varies from 10 to 30. The filter is based on a pixel-wise adaptive Wiener method based on statistics estimated from a local neighborhood of each pixel. The difference can already be seen in the profile to treat. A comparison between no filter, a filter of 10 and 30 pixels is presented in Figure 21. One can clearly see that the raw chemiluminescence signal contains high-frequency noise. This noise will lead to erroneous results as far as inverse Abel transform is concerned. On the other hand, a filter with a 30 kernel seems to damp too much the low-frequency changes observed in the signal. Those low-frequencies phenomena may come from combustion

This document is provided by JAXA.

and therefore shall be kept.

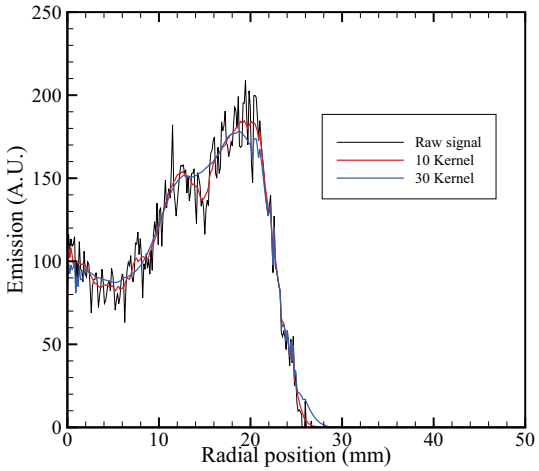

Figure 21: Effects of kernel size on raw signal

Therefore, for the following data, only a kernel size of 10 pixels by 10 pixels will be used to compute the planar chemiluminescence emission.

A typical difference of integrated results (Figure 22(a)) and Abel inverted result (Figure 22(b)) is presented.

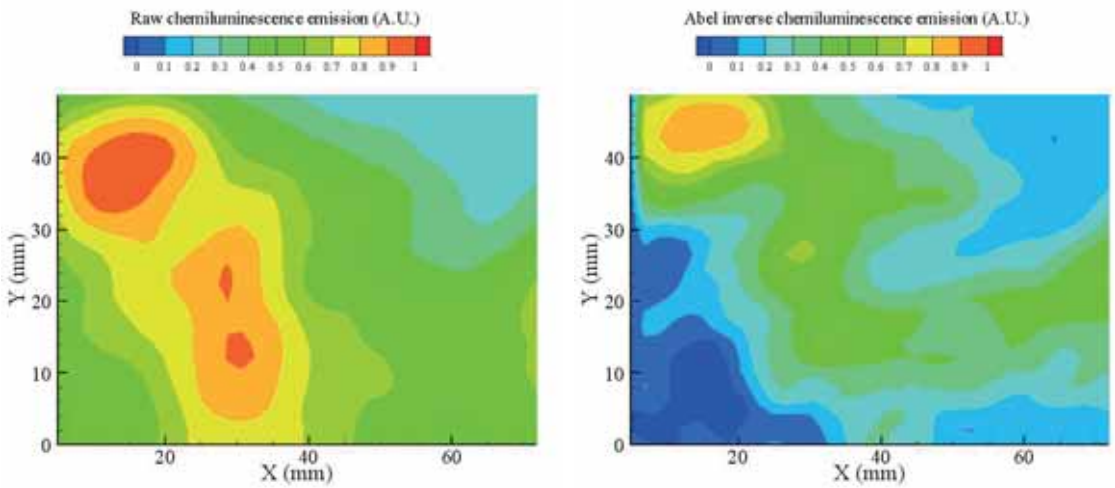

(a) Raw chemiluminescence image (b) Subsequent Abel inverted image

Figure 22: Phase delay of 0° for combustor #2 and $\phi = 0.50$: oscillating frequency 250Hz

This example clearly illustrates the importance of using Abel inverted images. One can see that the zone for which intense emission is detected is much smaller than in the raw image and closer to the exit of the swirler.

Another important parameter prior to compute a Rayleigh map is to estimate the pressure levels. The exact definition of the Rayleigh index is

This document is provided by JAXA.

$$R(x,y) = \frac{1}{\tau}\int_{\tau} p'(t,x,y)\cdot q'(t,x,y)dt \tag{9}$$

which requires the knowledge of both fluctuating pressure (p') and fluctuating heat release (q') in all points of the combustor. In practice, one assumes a spatially uniform pressure field in the imaging area for each phase. This hypothesis can be justified by the fact that the present instabilities are coming from a longitudinal mode (quarter wavelength) and that the pressure fields oscillate in phase. Furthermore, results presented in [16] clearly showed that this hypothesis can be made. As heat release can not be measured, one has to assume that heat release and chemiluminescence are proportional to each other. The exact level of the pressure signal may not be obtained and therefore, one may rather determine the degree of coupling between pressure and chemiluminescence rather than the value of the product:

$$R(x,y) \sim \frac{1}{\tau}\int_{\tau} p'(t)\cdot I'_{OH^*}(t,x,y)dt \tag{10}$$

Therefore in practice, the coupling is determined at each point and divided by the value that would result from a perfect coupling (sinusoidal changes in phase). This value is contained between -1 (phase of 180°) and 1 (perfect phase matching) and is called correlation between pressure and chemiluminescence.

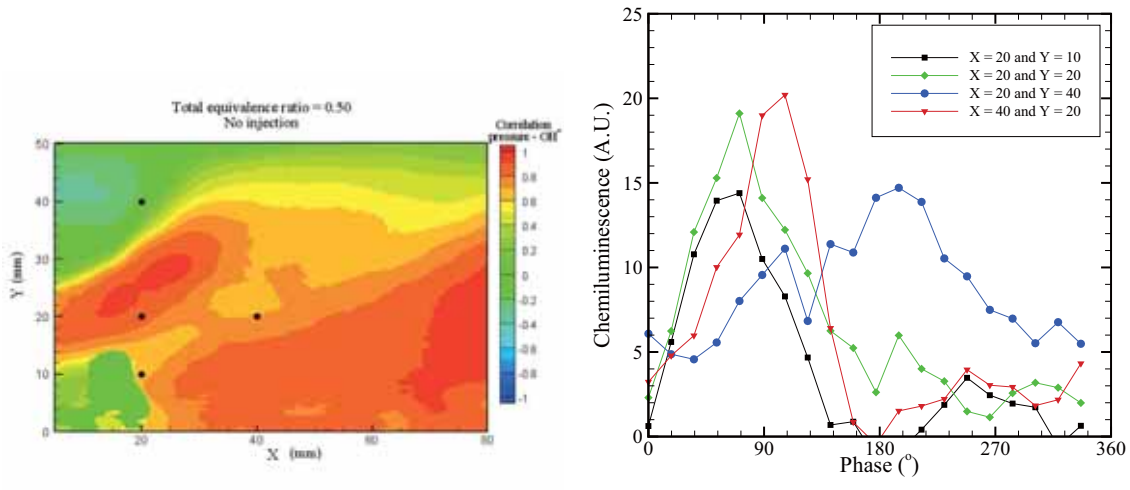

(a) Spatial correlation map

(b) Fluctuations of chemiluminescence at four different point for $\phi = 0.50$

Figure 23: Correlation between pressure-chemiluminescence in combustor #2 for $\phi = 0.50$: oscillating frequency 246Hz

The results for natural oscillations in combustor #2 are shown in Figure 23(a). One can see mainly two different regions having a correlation close to unity. The first region corresponds to the exit of the incoming mixture. The other one is linked with the recirculation. The flame presents a transition of structure, from the inverted-conical flame to the rim flame occurred between $\phi = 0.49 - 0.50$. A strong coupling in the first

This document is provided by JAXA.

region may come from upstream modifications of the incoming mixture due to pressure oscillations. In fact, it has been shown [17] that the equivalence ratio is modified due to the strong pressure oscillations and that for an overall mean equivalence ratio of 0.50, the actual equivalence ratio varies between 0.48 and 0.52, with a minimum for a phase of 135° and a maximum for 225°.

To illustrate further this tendency, the fluctuations of chemiluminescence at four different points within the previous image are shown in Figure 23(b). One can clearly see that the fluctuations of chemiluminescence at X=20,Y=40 are shifted with respect to other points. As shown in the spatially resolved map, this point is not strongly influenced by thermo-acoustics oscillations as correlation is close to zero.

This section showed the different data obtained through imaging techniques. The results clearly emphasized the importance to localize the regions of strong coupling between chemiluminescence and pressure to provide directions as far as active control is concerned. Next developments will deal with spectrally resolved data.

This document is provided by JAXA.

7 Results with spectrally resolved chemiluminescence

7.1 Detailed analysis of spectra

Spectral analysis of the flame offers very easy but however very fruitful information on the combustion mode. It is known that lean premixed combustion will mainly create OH* radicals and that radicals such as CH* and C_2^* will be very limited. To illustrate the lean premixed behavior, mean spectra are taken within oscillating combustion. The spectrometer used is the MS257 from Oriel coupled to an ICCD from Andor technology (DH534-18F-03 1024×1024 pixels). The ICCD is used in gate mode with an exposure of 60μs (which corresponds to values lower than 6° for oscillating combustion), intensification of 255 and a slit of 150μm. Full vertical binning is performed and accumulation over 1,000 samples is taken for each point. For those measurements, a series of two lenses was used. The lens was placed perpendicular to the combustor with a focal point in the center of the combustor, 100mm in the streamwise direction as well as in the transverse direction from the center. The fact that mainly OH* is

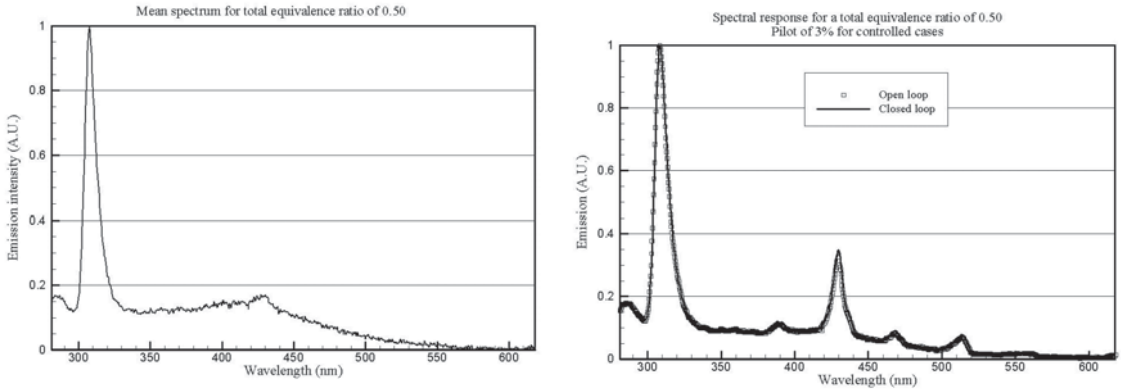

(a) Typical spectra for lean premixed flame for $\phi = 0.50$

(b) Typical spectra when using active control for $\phi = 0.50$

Figure 24: Spectrally resolved chemiluminescence without and with secondary injection for controlled cases.

visible for lean premixed combustion is perfectly shown in Figure 24(a), for which the overall equivalence ratio taken was fixed at 0.50, without any pilot. The absolute value of the intensity of the signal is not taken into account and therefore only a relative intensity is shown on the left axis. One can notice the OH* peak around 306nm and one may distinguish around 431nm a secondary peak, induced by CH* radicals, even though its value above the background is not very intense. C_2^* radicals are not visible for such lean conditions. On the other hand, looking at controlled cases through a secondary injection of fuel, one can notice the appearance of strong CH* (431nm and 387nm) and C_2^* emission (around 473 and 516nm) as shown in Figure 24(b). This is a clear indication of the diffusion process induced by the injection of the pilot. This

This document is provided by JAXA.

may has, as a consequence, strong effects on nitrous oxide emissions and therefore, for completing active control schemes, it is important to check the possible increase in NOx levels induced by this diffusion flame.

For active combustion, one may look more for temporal information to see changes within the combustor. Therefore, the next part presents typical temporal results obtained.

7.2 Determination of operating point control

To have a minimum of pollutant emission as well as a safe margin compared to blow off or oscillating combustion, the exact equivalence ratio should be known at any time. However, in gas turbines, the exact amount of air supplied is not precisely known and variations in the fuel properties may also affect the actual stoichiometry. Therefore, it is of practical importance to have a real time monitoring of this quantity. However, gas turbines are harsh environment and therefore, non-intrusive techniques are preferable. Some studies have shown that it may be possible to record incoming equivalence ratio using absorption techniques ([18]). However, again problems may come from long terms use of laser source and the influence of oscillations may not be negligible. Therefore, chemiluminescence was chosen but whereas many studies reported before ([10], [19], [20]) used spectrometer (low time resolution) the present sensing device can have higher temporal measurements.

Chemiluminescence is measured through a system of lens with a focal length of 300mm. The light exiting the lens is sent, through an optic fiber to a specbox (Hamamatsu, Inc.). This divides afterwards, through a series of band-pass filter and mirrors to four different photo-multipliers. The optical properties of each band-pass filters as well as the radical measured are shown in Table 1. It is worth noting that the two last wavelengths are representing the background emission in lean premixed flames, as it has been shown that C_2^* radicals can hardly be detected for typical stoichiometry below 0.90 [8]. The measurement is resulting from the integration over a volume and therefore no fine spatial resolution can be obtained. It has been shown in [21] that monitoring the ratio of (OH^*-background) / (CH^* - background) lead to an indication of the actual stoichiometry. To validate the presented approach (use of 3 different PMT rather than one spectrometer for a considerable gain in the frequency domain), measurements are also performed inside the target combustor. It is a swirl-type stabilized flame, having 12 vanes of 30° of angle each. The dimensions of the combustor are 100×100mm for the section and a total length of 210mm, extensible to 810mm to change the acoustic frequencies. An important feature is the presence of secondary injection orifices that may be used for active control strategies. The calibration is done without injecting the secondary fuel, considering only premixed methane-air flames. The location of the lens is at 20mm from the exit of the swirl, along the centerline of the combustor. Typical variable are inlet temperature and inlet velocity. The measured ratio is obtained using three different photo-multipliers, each having different voltage. The voltage is actually corrected to obtain a more uniform relation. Calibration was performed for a velocity of $30 m \cdot s^{-1}$, pre heated at 700K. One can notice on Figure 25(a) that the initial slope (for equivalence ratio (E.R.) below 0.5) is very steep, meaning that small changes in the stoichiometry leads to strong changes in the ratio between OH^* and CH^*. The background is removed on both signals (using PM3, emission between 471 and 475 nm). The results presented here are mean results obtained over 10s.

This document is provided by JAXA.

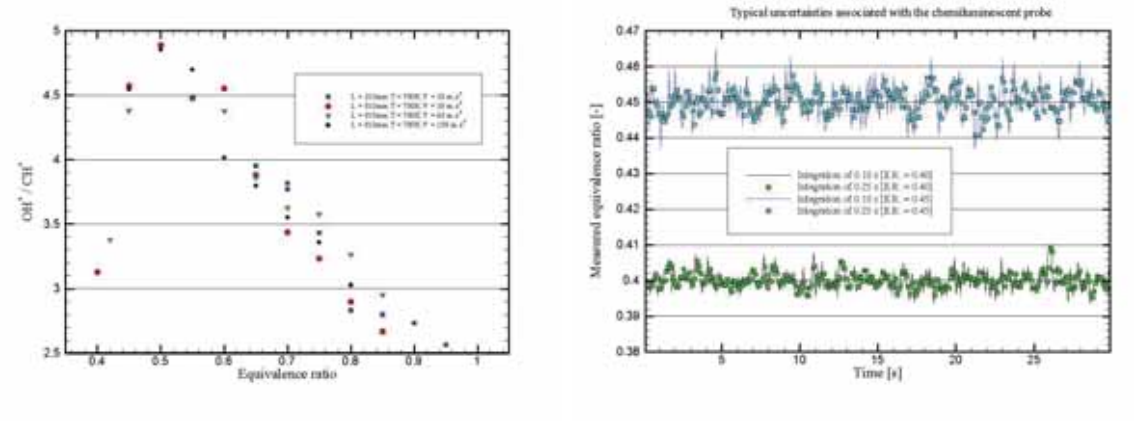

(a) Chemiluminescent ratios in demonstration combustor

(b) Time series evaluation of stoichiometry

Figure 25: Determination of the operating point control using ratio OH^*/CH^*

This is very interesting as the lean blowout limit lies within 0.4 and 0.45 depending on the velocity chosen. One can notice that the length of the combustor, affecting strongly the inner acoustics has no influence on the ratio. The actual ratio is non-monotonic, as also obtained through the numerical simulations of the chemiluminescence emission (see Section 2). The value for which the emission ratio is maximum slightly differs between experimental ($\phi = 0.48$) and numerical ($\phi = 0.44$) results (as shown previously in Sec. 2). The difference may come from uncertainties in the measurements due to relatively low emission levels or from the constant used to compute emission. However, in the region where blowout may occur (less than $\phi = 0.5$), the shape is monotonic, leading to non-ambiguous results.

Another point consists in determining the typical temporal response and accuracy of this measurement. The bulk velocity is set to $30\text{m}\cdot\text{s}^{-1}$, pre-heated at 700K. The value of the blowout is $\phi = 0.38$ for this case. This is illustrated in Figure 25(b), where two sampling rates are considered (10Hz and 4Hz). The imposed equivalence ratio is respectively 0.40 and 0.45. One can notice that the measured equivalence ratio (inferred from measured chemiluminescence ratio) is in good accordance with respect to the imposed one. Measuring the typical deviations as function of the sampling frequency gives an idea of the uncertainties. The results are displayed in Figure 26 where windows from 0.1 to 0.5s (frequencies between 2 and 10Hz) are considered for three different stoichiometry. One can see that taking windows of 0.1s to measure the equivalence ratio through chemiluminescence ratio gives raise to typical uncertainties of the order of 0.01 to 0.02 (which may represent 4%). The highest errors are found for equivalence ratio around 0.45, because it has been shown that the OH^*/CH^* is very sensitive in this region. Using lower sampling frequency (5Hz or 3.33Hz) enables to reduce drastically the uncertainties to levels below 3% for the different cases shown here. The uncertainty is computed as being the measurements of the relative fluctuations around the averaged value or root mean square. This is justified as steady mixture is used for those tests.

This document is provided by JAXA.

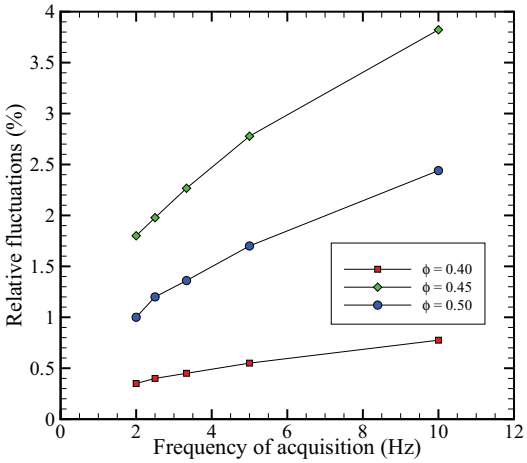

Figure 26: Typical uncertainties for lean premixed flames as function of acquisition frequency

In this section, it has been shown that taking the ratio of chemiluminescent species can yield the information concerning the burning equivalence ratio. This information may be used for low frequency (of the order of a few Hertz) loop control of the operating point. The main difference with previously published paper is that high frequency acquisition is also possible using this probe and the next section deals with this subsequent advantage compared to spectrometer with lower temporal possibilities.

8 Results with temporally resolved techniques

8.1 Simultaneous measurements of chemiluminescence-pressure for instability characterization

8.1.1 Time series Rayleigh

For active control strategies, it is very important to have sensors that can give in a very short time the appearance of self-sustained oscillations. Pressure signals is of course very efficient for this target, but the increase of pressure fluctuations are the results of the oscillations, not the cause. As known, it is the fact that heat release and pressure fluctuations are in phase that will provide energy to the oscillations, hence re-enforcing them and increasing the levels of pressure, which will in turn increase the levels of energy. Therefore, it seems more appropriate to try to measure the concordance of heat release rate versus pressure fluctuations with a good temporal resolution. The true Rayleigh index definition is the integral over one cycle and for the complete volume of pressure fluctuations times heat release fluctuations. This term is not easily obtained experimentally. Therefore, a slightly different expression is used in the following of this article (see equation 9 and 10).

Computing a mean Rayleigh index (sum of pressure fluctuations times heat release fluctuations over 1 second along the volume of the lens integration), one can see a strong relation between this mean value and the mean pressure fluctuation levels inside the combustor, as depicted by the graph represented in Figure 27(a).

For clarity reason, the logarithmic value (base 10) of the Rayleigh index is plotted on

This document is provided by JAXA.

the right side as a function of equivalence ratio. The pressure fluctuations are plotted as RMS values in kPa on the left side of the graph. One can clearly see that for low values of pressure levels, the computed Rayleigh index is negligible. For pressure levels of 0.7 to 0.75 kPa (which corresponds to equivalence ratio of 0.65 and 0.66 respectively), one can notice an increase of the Rayleigh index from 1 to 2 (which corresponds to one order of magnitude in absolute value). Afterwards, for a stoichiometry of 0.67, one can see that the pressure fluctuations reached a level of 1.52 kPa (two times higher than for $\phi = 0.66$). The Rayleigh index increase again from 2 to 6.5. Hence, it seems possible to gain more information using the Rayleigh index than only pressure fluctuations to see the possible appearance of acoustics oscillations. A small increase in pressure can result in high increase in correlation between pressure and heat release, which will lead to self-sustained oscillations.

The previous conclusion is valid for temporally stable situations. However, an important issue is the dynamics of the oscillations and to check if the Rayleigh information can provide faster results than just pressure levels considerations. Therefore, high sampling frequency (50kHz) is acquired and time-series measurements are analyzed to discuss this possibility. In Figure 27(b), a typical temporally resolved event is depicted (for which the origin of time is arbitrary chosen). It is important to understand that for lean cases, CH* may lead to low SNR and therefore OH* is favored. However, when stoichiometry is higher, CH* may be used and it is preferred as OH* is known to be also representative of hot regions, not only of flame front (see for instance Figure 24(a)).

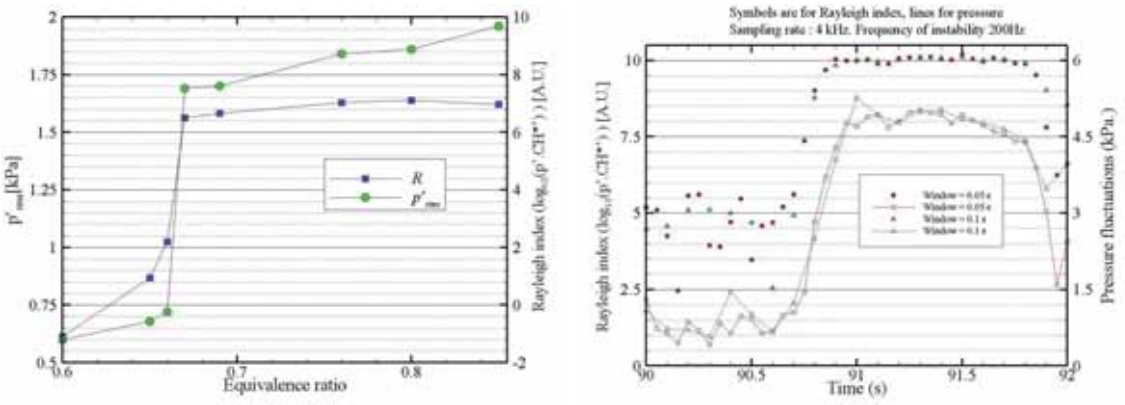

(a) Relation between Rayleigh index and pressure fluctuations

(b) Time series Rayleigh index(filled symbols) and pressure levels(open symbols).

Figure 27: On-line computing of Rayleigh index and its comparisons with pressure signal

The pressure fluctuations are displayed on the right axis in kPa and with open symbols, whereas the Log10 of the Rayleigh index is shown on the left axis with filled symbols. Two different integration times are considered, respectively 0.05 and 0.1s during which both pressure fluctuations and Rayleigh are computed. Therefore, there are twice more points for integration time of 0.05s (20Hz) rather than 0.1s (10Hz). One can notice that for time earlier than 90.5s, the pressure fluctuations remain limited to

This document is provided by JAXA.

levels lower than 1.5kPa, the Rayleigh index having values around 5. For a time of 90.75s, the Rayleigh index computed at 20Hz has a value of 7.5, which, as the scale is logarithmic constitutes a huge difference compared to previous levels around 5. On the opposite, for the same time, the pressure levels remain limited to 1.5kPa, which level was already reached before without leading to a sudden increase of the pressure levels inside the combustor. The next pressure sample rises to 3kPa whereas Rayleigh index rises to 9. This is clearly the appearance of strong self-induced oscillations, as previously reported in Figure 27(a). Through this example, it has been shown that using Rayleigh index as criteria for precursors of strong oscillations may result in a temporal gain of 0.05s, corresponding to 10 cycles. The reason for the emergence of an increase in the Rayleigh index is that heat release is phase-locked with pressure fluctuations prior to the increase of pressure levels. Therefore, for active controls strategies, one should also include a monitoring of the Rayleigh index. The decision to activate the active control may results in threshold on either pressure or Rayleigh levels. The actual transition will highly depend on the receiving optics of chemiluminescence (lens, fiber, photo-multiplies), so no general rule should be educed from the present experiments as far as levels are concerned.

8.1.2 Coherence

To further use the simultaneous information provided by the measurements of pressure and chemiluminescence, the spectral coherence is computed. The spectral coherence, in contrast to the Rayleigh Index (see Section 6.2) will no depend on the relative position of the pressure sensor with respect to the chemiluminescence measurements. The coherence is independent of phase information and aims at providing a measure of the matching in frequencies between two signals, like used for instance in [3]. Its mathematical definition may be given as

$$\gamma_{pE}(f) = \frac{|F_{pE}(f)|}{\sqrt{F_{pp}(f)F_{EE}(f)}} \tag{11}$$

Where F_{pE}, F_{pp} and F_{EE} denote the pressure-OH* cross-spectrum, the pressure power spectrum and the OH* power spectrum. Computing the coherence between pressure and chemiluminescence may provide information on the frequency coupling between the two quantities and on the effectiveness of the control algorithm. Values are bounded between 0 and 1, the latest showing a very strong coupling. Measurements are reported for three different cases in the final combustor and displayed in Figure 28. In this case, 65536 points were taken for both pressure and chemiluminescence to compute the spectra with a sampling frequency of 24kHz. All curves are obtained for an overall equivalence ratio of 0.50. The first curve (in red) corresponds to the case where all the fuel is injected in the mixing chamber and therefore for a second fuel percentage of 0. It is quite clear that strong coupling exists for frequencies of 235Hz, 470Hz and still relatively high level persist for higher frequencies like 705Hz. The second measurements are taken for steady-state injection of secondary fuel for an overall amount of 3% of the total fuel flow rate. The curve obtained is shown in green. One can see that even though a reduction in pressure could be obtained, the correlation between pressure and chemiluminescence remains high as shown by the coherence close to 1 for a frequency of 280Hz. This indicates that only a shift in frequency of the coherence could be obtained, but not a complete splitting between pressure and heat release. The coupling occurring

This document is provided by JAXA.

at a frequency for which pressure levels are lower than those observed at 235Hz may help explaining the successful reduction in pressure levels. Finally, using closed-loop control strategy (blue curve), one could obtain coherence levels lower than 0.80. It must be stated that the control strategy was focused on the 280Hz instability for which s coherence of only 0.55 is measured. This clearly shows the benefit of closed-loop controls, which enable a decoupling between pressure and heat release. On the other hand, for frequency domains away from the target frequency (like the 230Hz), coherence may become larger. A further reduction may be obtained if the control would also be able to decouple heat and pressure for frequency.

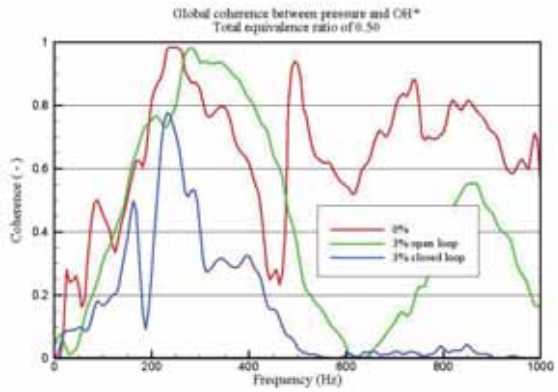

Figure 28: Coherence between pressure and OH* for no control, steady injection and closed-loop control cases

It turns out that coherence (which is not depending on phase, hence space) is a useful tool for diagnostics when dealing with instabilities. One may also think of developing an active control strategy based on the on-line measurements of this quantity to directly control the actuator.

8.2 Using time series to build controller

The development of proper controller is a very important task. However, trial and error procedures may be inappropriate as they may lead to severe problems. Predicting the effects (positive or negative) of a secondary injection of fuel is very important to reduce the development time.

8.2.1 Dynamic calibration of actuators

An important aspect of chemiluminescence measurement is that it allows temporally resolved diagnostics of combustion. It is therefore a very useful tool to evaluate transient combustion process. In an active control loop, one important aspect is the actuator response time and its influence on the main combustion. If detailed knowledge are known concerning the actual combustion and duration of the secondary injections system, it is afterwards easier to model the action of the actuator and to predict the best performances prior to real testing where pressure levels may be very important, limiting the number of trials.

This document is provided by JAXA.

The first aspect is to measure accurately the time lag between the command of the actuator and its real effect on combustion. For this purpose, the signal of the valve is changed from frequency of 250Hz to a frequency of 260Hz. Recording both the command signal and the chemiluminescence signal allows a precise determination of the time lag between command and actual influence on combustion. The tests performed showed an actual time lag of 72ms. The next aspect is to quantify the time lag between injection and reaction as function of both frequency and duration time of valve opening. It has been shown that control may be achieved even using sub-harmonic injection ([22]). One of the main reasons is that typical gaseous actuators have a better response for lower frequency and therefore the injection of gas is better controlled, providing a better shape for the heat release. Chemiluminescent measurements were done, recording the time series heat release due to secondary injection system. The total equivalence ratio at 0.52 with a secondary injection percentage of 22.2%.

Typical frequencies were ranging from 40 to 400 Hz whereas opening time was set at its lowest at 0.6 ms and the maximum depending on actuating frequency. CH* emission was recorded during the cycles of injection and the mean trace over 10 seconds are displayed in Figure 29 as function of both frequency and opened time. The averaged chemiluminescence signal within one period is represented. Different kind of signal can be sent to the actuator but in the following only step command (TTL) are investigated, providing a sharper signal than for instance a sinusoidal signal. One can notice that the traces obtained at lower frequencies are closer to a step than the one obtained at higher frequencies. One can also notice that the background emission is increasing with an increase of frequency, meaning the actual effects of the secondary injection are much smaller.

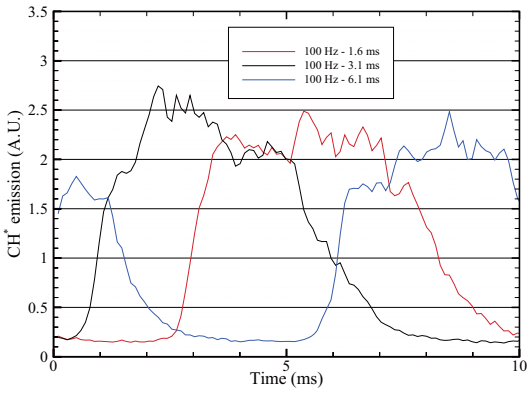

(a) Chemiluminescence measurements for a valve at 100 Hz

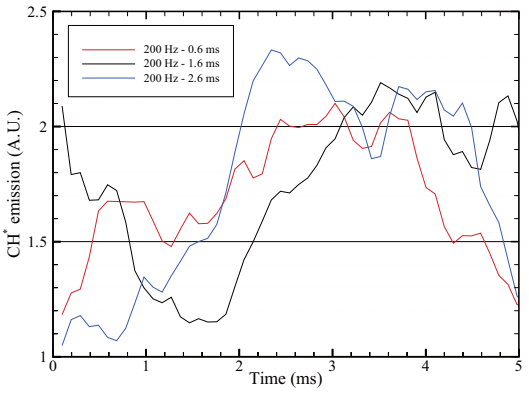

(b) Chemiluminescence measurements for a valve at 200 Hz

Figure 29: Real characteristics of secondary injection

This may come from the fact that the valve cannot completely be closed during one cycle and the percentage of fuel continuously injected becomes non-negligible. Having traces of heat release and the typical time lag between the command and the detection of the effect induced by the injection, it is possible to predict the effect of secondary injection on damping (or increasing) oscillations. Simulations are done by assuming a

This document is provided by JAXA.

perfect sinusoidal signal for the pressure fluctuations, as shown in Figure 30(a) having only one frequency.

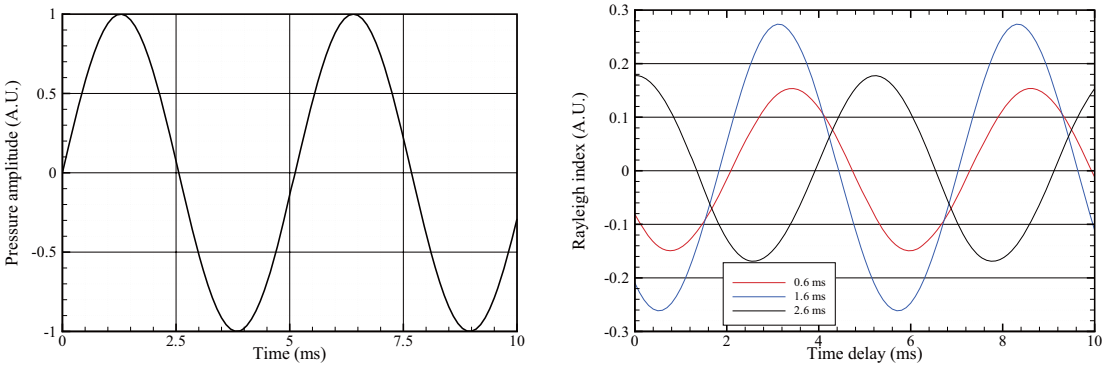

(a) Theoretical pressure fluctuations

(b) Theoretical Rayleigh estimation of the different configurations

Figure 30: Comparisons between predicted and measured efficiency

This approach is similar to the one adopted in ([19]). However, one of the main changes is that different frequencies for the valve are simulated to check a priori the best configuration possible. For each condition, a Rayleigh index may be computed assuming that there is a linear dependency between CH^* and heat release. This is simply done by integrating the pressure fluctuations and the heat release fluctuations over one cycle. Pressure fluctuations are assumed to be sinusoidal as shown in Figure 30(a). Typical results obtained are summarized in Figure 30(b) when simulating instability at 200Hz and controlling it with a secondary injection pulsing at 200Hz also. Three different valve opening times are compared (0.6, 1.6 and 2.6ms) and the Rayleigh index is computed.

8.2.2 Predicting control results

The lowest values are obtained for an opening time of 1.6ms at a time delay of 0.5ms after a positive slope in the pressure signal is detected. It is also important to notice that a bad phase delay will re-enforce the actual instabilities, as a positive Rayleigh index is computed for instance for the same opening command but with a delay of 3ms. This means that at least two variables (time delay and opening command) have to be optimized simultaneously to damp oscillations. In practice, there may be another factor to adjust: the actual frequency of the valve. In theory, the optimal frequency of control is the frequency of oscillations. However, for high frequencies instabilities, it may be possible that lower actuating frequencies will damp more the oscillations. Simulations for a frequency of 200Hz are displayed in Figure 31 for control frequency of 200 and 100Hz respectively.

In this case, the best time delay between pressure and heat release is chosen and the results are only plotted with respect to opening time and frequencies of valve. One can see that the best damping performance is obtained for an injection of 200Hz

This document is provided by JAXA.

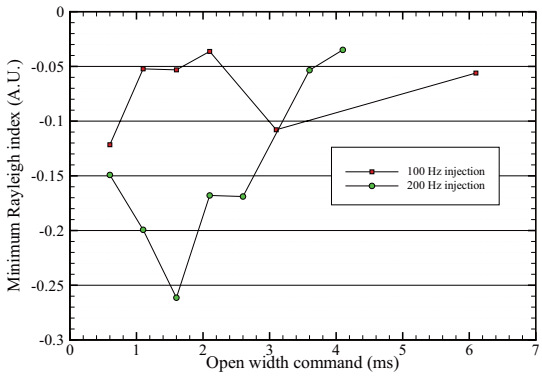

Figure 31: Predicted reductions of acoustics oscillations

whereas lower harmonics such as 100Hz still shows good results. It is worth noting that using lower injection (100Hz) would allow damping only one third as compared with harmonic injection for this specific case. Therefore, as long as the shape can be well controlled, one should use harmonic injection for active control strategies. The best results of the model for a thermo-acoustic instability with a frequency of 200Hz are hence obtained for a harmonic injection with an opening command of 1.6ms and a time delay around 0.5ms between the positive slope of the pressure and the TTL sending command. The next section shows actual comparison between the predictions and measurements performed in the demonstration combustor.

8.2.3 Comparisons with experiments

To validate the model, experiments are carried out. The percentage of secondary fuel was set to 14.25% and the total equivalence ratio was 0.88. In combustor #1 this condition corresponds to high pressure oscillations. To validate the model, the time delay as well as open width command is varied and pressure signals are measured. The typical frequencies measured are 220Hz, so the valve is operated at the same frequency. The first tests deal with the influence of time delay for a command of 1.6ms. The delay is varied from 0 to 3ms. The pressure amplitudes without control were 2.54kPa for an overall equivalence ratio of 0.85 and 0.90. The results are presented in Figure 32(a) where the modeled Rayleigh index is shown in the right side of the graph and the measured pressure fluctuations levels are shown on the left side. One can notice that both data show a minimum for a delay around 0.5ms and then increase for higher and shorter delays. The fact that the two curves do not perfectly overlap may come from the fact that the frequency of the model was 200Hz and the real one 220Hz. The second reason is that the tests of the valve were not performed exactly at the same condition of mass flow rate (hence velocity of secondary injection). However, the general behavior is obtained through the previously exposed model. Another series of tests consist in determining the best open width command for a fixed delay with respect to pressure signal. The results are shown in Figure 32(b), where the delay with respect to pressure is fixed at 0.4ms. The open command is changed from 0.6 to 2.1ms in the experiments and to 3.6 in the modeled data.

One can again notice that similar trends are found on both the experimental results and the results obtained though the model. The optimum point obtained experimen-

This document is provided by JAXA.

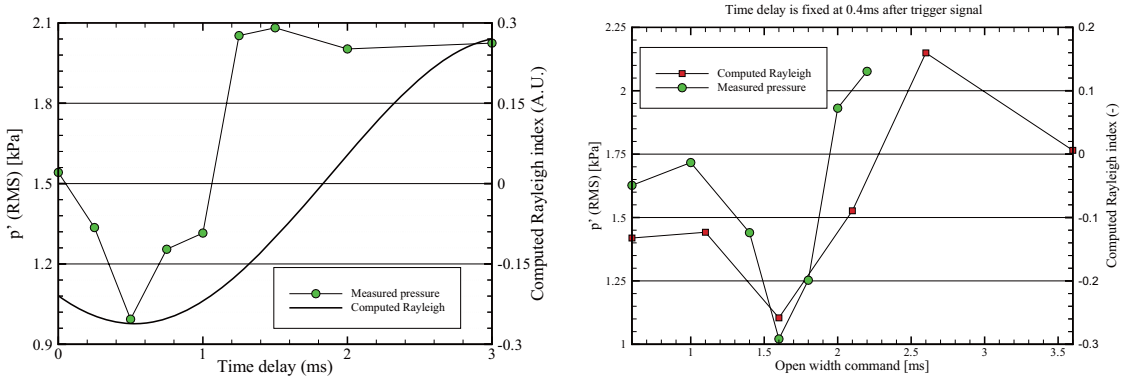

(a) Effects of time delay for an opened time of 1.6ms

(b) Effects of opened time for a delay of 0.4ms

Figure 32: Comparisons between predicted and measured efficiency

tally corresponds to the predicted one. Hence, it seems possible to take benefit of the validity of the model to predict the behavior of the active control loop. It may result in initial conditions close to the optimum one and therefore be a good start for an active control loop with adaptive output to match time varying inputs. Therefore, the model and the chemiluminescent measurements required as input are good tools for active control strategies, especially concerning the development of algorithm.

This section showed the different data obtained by time resolved chemiluminescence and its implementation for active control loop strategies.

9 Conclusions

Different applications of chemiluminescence were presented and their applications to understand oscillating combustion and its control were discussed. Even though chemiluminescence remains a qualitative quantity, its measurement is a key point in the application of active control of combustion. A detailed description of Abel inversion schemes and its resultant uncertainties has been shown to validate the hypothesis when using a 105mm focal length lens. Applications of chemiluminescence in two different combustors showed different characteristics of premixed or partially premixed turbulent combustion. The use of spatially resolved techniques enabled to locate the regions where coupling between pressure and heat release was strong through the use of a correlation map between Abel inverted chemiluminescence map and pressure . This is important for active control schemes as it shows the typical mechanisms to eliminate towards effective control. The use of spectrally resolved approach offered a double potential. The first was to describe the nature of the flame (fully premixed or not) through the appearance of C_2^* emissions when using secondary injection schemes compared to a fully premixed case. The other application is to monitor the ratio of OH^* versus CH^* to estimate the operating point control. This approach was also validated

This document is provided by JAXA.

through some numerical simulations of chemiluminescence. It was shown that the ratio is monotonic for ultra-lean mixtures but non-monotonic around an equivalence ratio of 0.50 for preheated mixtures at 700K. For all cases, a good estimate could be reached with a sampling frequency of a few Hz. Finally, the temporally resolved approach enabled to estimate precursors of thermo-acoustics instabilities through the coupling between pressure and chemiluminescence, this coupling becoming high just before the appearance of strong pressure levels. Finally, the usage of coherence proved to be a good tool for active control strategy by showing the frequencies for which coupling is still existing, providing further data for the controller.

Controller of next generations may include all those different aspects, and one may have different control-loops. Relatively low frequencies will be required for adjusting the operating point control, whereas high frequencies are necessary to couple with thermo-acoustics instabilities and their reductions. Next research themes will include the development of such algorithms and great care should be taken in considering uncertainties linked with each sensor and the controller should be able to handle apparently conflicting information from two different sensors.

References

[1] B.T. Zinn and T.C. Lieuwen. Combustion instabilities in gas turbine engines: Operational experience, fundamental mechanisms, and modeling. volume 210, chapter Combustion instabilities: basic concept. Progress in Astronautics and Aeronautics, 2005.

[2] S. Candel. Combustion dynamics and control: Progress and challenges. *Proc. Combust. Inst.*, 29:1–28, 2002.

[3] J. Anthoine, M. Mettenleiter, O. Repellin, J-M. Buchlin, and S. Candel. Influence of adaptive control on vortex-driven instabilities in a scaled model of solid propellant motors. *J. Sound Vib.*, 262:1009–1046, 2003.

[4] A. Wachsman, S. Park, Z.C. Sobhani, A.N. Annaswamy, and A.F. Ghoniem. Simultaneous combustion instability and emissions control using air and fuel modulation. In *AIAA-2004-633, 42nd AIAA Aerospace Sciences Meeting and Exhibit, Reno, Nevada, Jan. 5-8, 2004*, 2004.

[5] S.T. Sanders, D.W. Mattison, J.B. Jeffries, and R.K. Hanson. Sensors for high-pressure, harsh combustion environments using wavelength-agile diode lasers. *Proc. Combust. Inst.*, 29:2661–2667, 2002.

[6] L.Zimmer, S. Tachibana, M. Tanahashi, M. Shimura, and T. Miyauchi. Sensors for active control of combustion. In *Proceedings of the 6th Symposium on Smart Control of Turbulence*, pages 163–172, 2005.

[7] N. Docquier and S. Candel. Combustion control and sensors: a review. *Prog. Energ. Combust.*, 28:107–150, 2002.

[8] J. Kojima, Y. Ikeda, and T. Nakajima. Basic aspects of OH(A), CH(A), and C2(D) chemiluminescence in the reaction zone of laminar methane-air premixed flames. *Combust. Flame*, 140:34–45, 2005.

[9] T.M. Muruganandam, B.-H. Kim, M.R. Morrell, V. Nori, M. Patel, B.W. Romig, and J.M. Seitzman. Optical equivalence ratio sensors for gas turbine combustors. *Proc. Combust. Inst.*, 29:1601–1609, 2002.

This document is provided by JAXA.

[10] N. Docquier, F. Lacas, and S. Candel. Closed-loop equivalence ratio control of premixed combustors using spectrally resolved chemiluminescence measurements. *Proc. Combust. Inst.*, 29:139–145, 2002.

[11] S. Tachibana, L. Zimmer, Y. Kurosawa, K. Suzuki, J. Shinjo, Y. Mizobuchi, and S. Ogawa. Active control of combustion oscillations in a lean premixed combustor by secondary fuel injection. In *Proceedings of the 6th Symposium on Smart Control of Turbulence*, pages 181–190, 2005.

[12] C. J. Dasch. One-dimensional tomography: a comparison of abel, onion-peeling, and filtered backprojection methods. *Appl. Optics*, 31:1146–1152, 1992.

[13] G. Singla, P. Scouflaire, J. Rolon, and S. Candel. Transcritical oxugen/transcritical or supercritical methane combustion. *Proc. Combust. Inst.*, 30:2921–2928, 2005.

[14] A. F. Ghoniem, A. Annaswamy, S. Park, and Z. C. Sobhani. Stability and emissions control using air injection and H2 addition in premixed combustion. *Proc. Combust. Inst.*, 30:1765–1773, 2005.

[15] B. Taupin, D. Vauchelles, G. Cabot, and A. Boukhalfa. Experimental study of lean premixed turbulent combustion. In *11th International Symposium on Applications of Laser Techniques to Fluid Mechanics, 8-11 July, Lisbon*, 2002.

[16] S. Tachibana, L. Zimmer, Y. Kurosawa, and K. Suzuki. Active control of combustion oscillations in a lean premixed combustor by secondary fuel injection coupling with chemiluminescence imaging technique. *Proc. Combust. Inst.*, 31:3225–3233, 2007.

[17] L. Zimmer and S. Tachibana. Laser induced plasma spectroscopy for local equivalence ratio measurements in an oscillating combustion environment. *Proc. Combust. Inst.*, 31:737–745, 2007.

[18] J. G. LEE, K. KIM, and D. A. SANTAVICCA. Measurement of equivalence ratio fluctuation and its effect on heat release during unstable combustion. *Proc. Combust. Inst.*, 28:415–421, 2000.

[19] J.G. Lee and D. Santavicca. Experimental diagnostics for the study of combustion instabilities in lean premixed combustors. *J. Prop. Power*, 19:735–750, 2003.

[20] T.M. Muruganandam, B.-H. Kim, M.R. Morrell, V. Nori, M. Patel, B.W. Romig, and J.M. Seitzman. Optical equivalence ratio sensors for gas turbine combustors. *Proc. Combust. Inst.*, 30:1601–1609, 2005.

[21] L.Zimmer, S. Tachibana, T. Yamamoto, Y. Kurosawa, and K. Suzuki. Evaluation of chemiluminescence as sensor for controlling lean premixed combustion. In *Proceedings of the 4th Symposium on Smart Control of Turbulence*, pages 93–102, 2003.

[22] E. Lubarsky, D. Shcherbik, A. Bibik, and B.T. Zinn. Open loop control of severe combustion instabilities by fuel flow modulation at non resonant frequencies. In *AIAA-2004-634, 42nd AIAA Aerospace Sciences Meeting and Exhibit, Reno, Nevada, Jan. 5-8, 2004*, 2004.

This document is provided by JAXA.

This document is provided by JAXA.

JAXA Research and Development Memorandum JAXA-RM-06-016E

Date of Issue : March 30,2007

Edited and Published by : Japan Aerospace Exploration Agency

7-44-1 Jindaiji-higashimach, Chofu-shi,Tokyo 182-8522,Japan

URL : http://www.jaxa.jp/

Printed by : NORTH ISLAND Co.,Ltd

Inquires about copyright and reproduction should be addressed to the Aerospace Information Archive Center, Information Systems Department, JAXA.

2-1-1 Sengen, Tsukuba-shi, Ibaraki 305-8505, Japan

Phone : +81-29-868-5000 Fax : +81-29-868-2956

Copyright © 2007 by JAXA.

All rights reserved. No part of this publication may be reproduced, stored in retrieval system or transmitted, in any form or by any means, electoronic, mechanical, photocopying, recording, or otherwise, without permission in writing form the publisher.

This document is provided by JAXA.

Printed on Recycled Paper

This document is provided by JAXA.